World Electric Vehicle Journal

MDPI

Article

Topology Optimization Design and Dynamic Performance Analysis of Inerter-Spring-Damper Suspension Based on Power-Driven-Damper Control Strategy

Jinsen Wang [1], Yujie Shen [1,*], Fu Du [2], Ming Li [3] and Xiaofeng Yang [4]

[1] Automotive Engineering Research Institute, Jiangsu University, Zhenjiang 212013, China
[2] Chinese Scholartree Ridge Laboratory, China North Vehicle Research Institute, Beijing 100072, China; 3120205202@bit.edu.cn
[3] Weichai (Yangzhou) Yaxing New Energy Commercial Vehicle Co., Ltd., Yangzhou 225000, China; liming@asiastarbus.com
[4] School of Automotive and Traffic Engineering, Jiangsu University, Zhenjiang 212013, China; yangxf18@ujs.edu.cn
* Correspondence: shenyujie@ujs.edu.cn; Tel.: +86-15050852025

Abstract: In this paper, the problem of broadband vibration suppression of power-driven-damper vehicle "inerter-spring-damper" (ISD) suspension is studied. The suspension can effectively inherit the low-frequency vibration suppression effect of ISD suspension and the high-frequency vibration suppression effect of the power-driven-damper control strategy. Based on the structural method, this paper proposes four suspensions with different structures. The optimal structure and parameters are obtained by using pigeon-inspired optimization. The results show that, based on the optimal structure, the Root-Mean-Square (RMS) of body acceleration and the RMS of suspension working space are reduced by 23.1% and 6.6%, respectively, compared to the traditional passive suspension. The influence of the damping coefficient on the dynamic performance of the power-driven-damper vehicle ISD suspension is further studied. The vibration suppression characteristics of the proposed suspension are simulated and analyzed in both the time domain and frequency domain. It is shown that the power-driven-damper vehicle ISD suspension can effectively reduce vibrations across a wide frequency range and significantly improve body acceleration and suspension working space, thereby enhancing the ride comfort.

Keywords: vehicle ISD suspension; power-driven-damper control strategy; ride comfort; inerter

check for updates

Citation: Wang, J.; Shen, Y.; Du, F.; Li, M.; Yang, X. Topology Optimization Design and Dynamic Performance Analysis of Inerter-Spring-Damper Suspension Based on Power-Driven-Damper Control Strategy. *World Electr. Veh. J.* **2024**, *15*, 8. https://doi.org/10.3390/wevj15010008

Academic Editor: Joeri Van Mierlo

Received: 9 November 2023
Revised: 19 December 2023
Accepted: 20 December 2023
Published: 26 December 2023

Copyright: © 2023 by the authors. Licensee MDPI, Basel, Switzerland. This article is an open access article distributed under the terms and conditions of the Creative Commons Attribution (CC BY) license (https://creativecommons.org/licenses/by/4.0/).

1. Introduction

The suspension system is a crucial component of the chassis structure. It is responsible for supporting the vehicle's weight and for absorbing and reducing the impact of vibrations caused by uneven road surfaces. The comprehensive performance of the suspension directly affects its ride comfort, handling stability, and driving safety. Therefore, the improvement of suspension performance is crucial [1–3]. The traditional passive suspension has been widely used due to its low cost and simple structure. However, its single structure limits the potential for improving the vibration isolation performance of the suspension system [4–6]. In 2002, Professor Smith proposed the concept of inerter, and the performance of passive suspension has since been further developed. The inerter is a mechanical component with two-end motion characteristics; its purpose is to compensate for the lack of mass impedance. It has been utilized in various fields, such as building vibration isolation and aircraft landing gear. In recent years, the structure of passive suspension has become more diverse with the introduction of inerter. We refer to the suspension with the core structure of "inerter-spring-damper" as ISD suspension. The introduction of the inerter has greatly expanded the topology of suspension, and the research on ISD suspension structure

has emerged endlessly [7–9]. Chen designed a two-stage tandem ISD suspension structure based on the electromechanical similarity principle [10]. Jiang constructed 12 suspension systems with inerter and utilized multi-objective optimization methods to optimize the suspension parameters. The simulation results show that, compared with traditional suspension, there are eight types of ISD suspension structures that exhibit better performance. Among them, four types of ISD suspension structures have significant vibration reduction effects [11]. Xie established eight types of ISD seat suspensions and analyzed the model's dynamic response across various frequency bands. The results indicate that seat suspension with inerter provide significant advantages in vibration isolation compared to traditional seats suspension. They have a notable effect on low-frequency vibration isolation, but their effectiveness is limited in the high-frequency range [12]. Nie proposed a new hybrid ISD suspension. Simulation results indicated that the structure could decrease the vertical weighted acceleration at the seat by 26% and significantly improve the ride comfort [13]. Papageoriou transformed the network structure design of suspension systems into the optimization solution for the positive real impedance transfer function and designed the suspension structure through the passive network synthesis theory [14]. Based on this, Jiang studied the structural realization of high-order impedance [15]. Zhang proposed a new a new method for suspension structure design called structural impedance method. This method can simultaneously consider a complete set of absorber layouts and limit the complexity, topology, and element values of the candidate layouts [16]. Vehicle ISD suspension has significantly improved its topological characteristics compared to traditional suspensions, and it can effectively suppress the body vibration in the low-frequency range, but it has poor vibration suppression effect in the high-frequency range and cannot effectively suppress vibration across a wide frequency range.

While the use of inerters can passively improve the dynamic properties of vehicles, semi-active suspension systems were developed to provide a more balanced compromise between cost and performance. In a semi-active suspension system, the damping force can be adjusted based on operating conditions to improve suspension performance [17–19]. Karnopp and Crosby first proposed the concept of semi-active suspension. Under the concept of semi-active suspension, a variety of excellent control strategies for semi-active suspension have emerged [20]. Karnopp proposed a skyhook (SH) control strategy to suppress body vibration by installing an adjustable damper on the sprung mass. This damper produces a damping force that opposes the velocity of the sprung mass [21]. Zhu applied the acceleration-driven-damper (ADD) control strategy to double crossarm suspension, and the research shows that the ADD control strategy can effectively suppress the body vibration [22]. Lin proposed an improved ADD control strategy; the research shows the improved ADD control strategy maintains the optimization effect of the ADD control strategy on sprung mass acceleration and prevents the deterioration of dynamic tire load [23]. Wang analyzed the SH control strategy and the liner-quadratic-regulator (LQR) control strategy, respectively, and he proposed SH-LQR semi-active control to improve ride comfort. According to the simulation results of the semi-vehicle model, the suspension utilizing SH-LQR control improves the body acceleration and pitch angle acceleration by 28.3% and 26.3%, respectively, compared to the passive suspension. Furthermore, the frequency domain analysis shows that the SH-LQR control strategy yields superior control effectiveness in both high and low frequency bands [24]. Savaresi proposed the SH-ADD control strategy, which combines SH control strategy and ADD control strategy, and the research shows that the control strategy an effectively improve the body acceleration in both high and low frequency range [25]. In order to achieve vibration suppression in both the high frequency and low frequency range, the current approach primarily relies on the method of hybrid control strategy design. However, the process of switching between these control strategies can lead to system instability and jitter.

The power-driven-damper control strategy is a semi-active control strategy designed from the perspective of system power requirements. Compared with the ADD control, the power-driven-damper control can effectively improve body vibration in the high-frequency

range without causing body shake [26]. Therefore, this paper combines the power-driven-damper control strategy, which can suppress the vibration in the high-frequency range, with the vehicle ISD suspension, which can suppress the vibration in the low-frequency range. The research focuses on the quarter suspension model and analyzes the impact of the power-driven-damper vehicle ISD suspension on the vertical motion of the vehicle.

2. Model Building and Power-Driven-Damper Control Strategy Design

2.1. Quarter Suspension Model

In this paper, a quarter suspension model based on the power-driven-damper control strategy is taken as the research object, as shown in Figure 1.

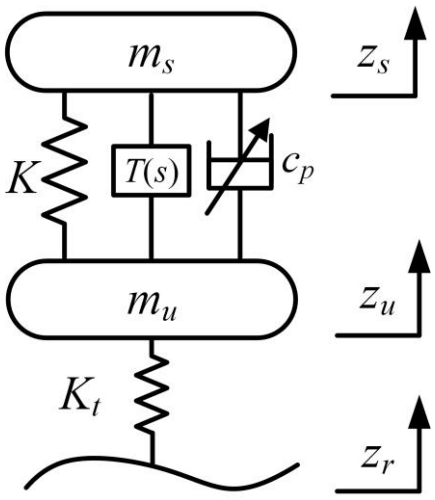


Figure 1. Quarter suspension model.

In the figure, K is the auxiliary spring, c_p is the semiactive damper, m_s is the sprung mass, m_u is the unsprung mass, z_s is the vertical displacement of the sprung mass, z_u is the vertical displacement of the unsprung mass, z_r is the random road input, K_t is the equivalent spring of the tire. $T(s)$ is an intermediate structure consisting of the inerter and springs. The dynamic motion equations of the suspensions are as follows:

$$\begin{cases} m_s\ddot{z}_s + K(z_s - z_u) + c_p(\dot{z}_s - \dot{z}_u) + T(s)(\dot{z}_s - \dot{z}_u) = 0 \\ m_u\ddot{z}_u + K_t(z_u - z_r) - K(z_s - z_u) - c_p(\dot{z}_s - \dot{z}_u) - T(s)(\dot{z}_s - \dot{z}_u) = 0 \end{cases} \tag{1}$$

2.2. Power-Driven-Damper Control Strategy Design

Port-controlled Hamiltonian system [27] is a mathematical framework that focuses on capturing the interaction between energy and power in a system's topology and characterizing the stored energy through Hamiltonian equation. The framework can be used to construct a variety of nonlinear models, such as robotic systems and electromechanical systems. At present, the research of the port-controlled Hamiltonian system focuses on obtaining a closed-loop port-controlled Hamiltonian system. This involves manipulating the power port to derive the corresponding Hamiltonian equation, power interaction equation, and damping parameters. For a generalized port-controlled Hamiltonian system, the dynamic behavior of the system can be described by Equation (2):

$$\begin{aligned} \dot{x} &= [J(x) - R(x)]\frac{\partial H}{\partial x}(x) + g(x)u \\ y &= g^T(x)\frac{\partial H}{\partial x}(x) \\ J(x) &= -J^T(x) \\ R(x) &= -R^T(x) \geq 0 \end{aligned} \tag{2}$$

where x is the state variable, y is the output variable, and u is the port power variable. $J(x)$ is the power interconnection matrix of the subsystem; $R(x)$ is the damping dissipation matrix.

The damping dissipation matrix reflects the damping dissipation energy relationship on the system port $H(x)$ is the Hamiltonian energy function of the system, which stores the energy in the system; $g(x)$ is a function that is associated with the state variable. $y^{\mathrm{T}}u$ represents the system power, which can be expressed by Equation (3):

$$y^T u = \frac{dH}{dt} + \frac{\partial H^T}{\partial x} R \frac{\partial H}{\partial x} \geq \frac{dH}{dt} \tag{3}$$

Part of the power input to the system is stored as energy, which is quantized by the Hamiltonian energy function $H(x)$. The other part is damped, dissipated, and quantized by the damping dissipation matrix $R(x)$. However, the direct effects of input variables on the dissipative matrix $R(x)$ and the interconnection matrix $J(x)$ have not been taken into account. In order to more accurately describe the electromechanical system using the port-controlled Hamiltonian system framework, we introduce the interconnection matrix $J(x,v)$ and the dissipation matrix $R(x,v)$. These matrices are related to both the input variables and state variables. And Equations (2) and (3) have been modified to derive Equations (4) and (5) as follows:

$$\begin{aligned} \dot{x} &= [J_1(x,v) - R_1(x,v)]\tfrac{\partial H}{\partial x}(x) + g(x,v)u \\ y &= g^T(x,v)\tfrac{\partial H}{\partial x}(x) - [J_2(x,v) - R_2(x,v)]u \\ J_i(x,v) &= -J^T{}_i(x,v) \qquad i = 1,2 \\ R_i(x,v) &= -R^T{}_i(x,v) \quad i = 1,2 \end{aligned} \tag{4}$$

$$y^T u = \frac{dH}{dt} - \frac{\partial H^T}{\partial x} R_1(x,v) \frac{\partial H}{\partial x} + u^T R_2(x,v) u \tag{5}$$

where v, as the input variable, represents controllable damping, $J_i(x,v)$ represents the power interconnection matrix, and $R_i(x,v)$ represents the power dissipation matrix. The total input power $y^T u$ consists of two parts: the first part is the stored power, and the second part is the dissipated power. The dissipated power is denoted as $d(v,x)$ in this paper, and it can be expressed by Equation (6). The corresponding power balance equation can be expressed as Equation (7).

$$d(v,x) = \frac{\partial H^T}{\partial x} R_1(x,v) \frac{\partial H}{\partial x} + u^T R_2(x,v) u \tag{6}$$

$$\dot{H} = y^T u - d(v,x) \tag{7}$$

From the perspective of system power demand, the design of semi-active control strategy based on power-driven-damper can be transformed into a problem of solving an input variable that satisfies the power demand of a port-controlled Hamiltonian system. This can be expressed by the following control methods:

$$v : \begin{cases} \operatorname{argmax}(\dot{H} + d) & \text{if} \operatorname{argmax}(\dot{H} + d) < W_d \\ \operatorname{argmin}(\dot{H} + d) & \text{if} \operatorname{argmax}(\dot{H} + d) \geq W_d \\ W_d = \dot{H} + d(v,x) & \text{otherwise} \end{cases} \tag{8}$$

Taking Figure 1 as an example, in the suspension system, the spring and the inerter are energy storage components, while controllable damping is the only energy dissipation component.

Therefore, the stored power is:

$$\dot{H} = K(z_s - z_u)(\dot{z}_s - \dot{z}_u) + T(s)(\dot{z}_s - \dot{z}_u)^2 \tag{9}$$

The dissipated power is:

$$d(c_p, x) = c_p(\dot{z}_s - \dot{z}_u)^2 \tag{10}$$

The total suspension system power is:

$$W_d = \dot{H} + d(c_p, x) = K(z_s - z_u)(\dot{z}_s - \dot{z}_u) + c_p(\dot{z}_s - \dot{z}_u)^2 + T(s)(\dot{z}_s - \dot{z}_u)^2 \quad (11)$$

The power-driven-damper control strategy is designed from an energy perspective. The closer the total power is to zero, the stronger its isolation of power. Therefore, the design rules for the control strategy in this paper are as follows: When the net input power in suspension is less than zero, c_p is set to its maximum value. When the net input power in suspension is greater than or equal to zero, c_p takes the minimum value; When the net input power of suspension is zero, but the relative displacement of suspension is not zero, (indicating that the relative speed is zero, but the relative displacement is not), c_p is taken as the average value between maximum and minimum values. This process is considered the transition stage. In the last mode, the c_p value ensures zero net input power. The power-driven-damper control strategy avoids the switching conditions associated with body acceleration and can effectively suppress shaking. The conditions that must be met for the controllable damping coefficient c_p are as follows:

$$c_p = \begin{cases} c_{\max}, if\ K(z_s - z_u)(\dot{z}_s - \dot{z}_u) + c_{\max}(\dot{z}_s - \dot{z}_u)^2 + T(s)(\dot{z}_s - \dot{z}_u)^2 < 0 \\ c_{\min}, if\ K(z_s - z_u)(\dot{z}_s - \dot{z}_u) + c_{\min}(\dot{z}_s - \dot{z}_u)^2 + T(s)(\dot{z}_s - \dot{z}_u)^2 \geq 0 \\ \frac{c_{\max}+c_{\min}}{2}, if\ (\dot{z}_s - \dot{z}_u) = 0 \& (z_s - z_u) \neq 0 \\ \frac{-K(z_s - z_u) - T(s)(\dot{z}_s - \dot{z}_u)}{(\dot{z}_s - \dot{z}_u)}, \text{else} \end{cases} \quad (12)$$

3. Topological Design and Dynamic Performance Optimization of Suspension Structure

3.1. Suspension Structure Topology Design

In this paper, the number of inerters is limited to 1. By connecting the inerter in series and parallel with different numbers of springs, a total of four types of power-driven-damper vehicle ISD suspensions with different structures are obtained, namely S1, S2, S3, and S4, as shown in Figure 2.

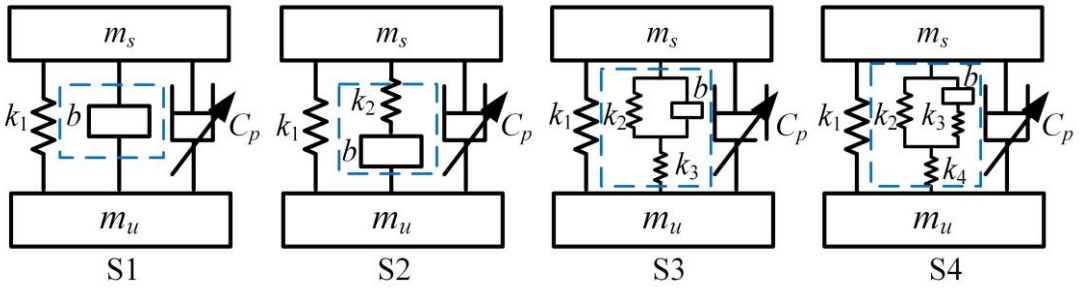


Figure 2. Four suspension structures.

The transfer function of the velocity impedance for these four intermediate suspension structures is:

$$\begin{aligned} T_{S1}(s) &= bs \\ T_{S2}(s) &= \frac{k_2 bs}{bs^2 + k_2} \\ T_{S3}(s) &= \frac{k_3 bs^2 + k_2 k_3}{bs^3 + (k_2 + k_3)s} \\ T_{S4}(s) &= \frac{bk_4(k_2 + k_3)s^3 + k_2 k_3 k_4}{b(k_2 + k_3 + k_4)s^3 + k_3(k_2 + k_4)s} \end{aligned} \quad (13)$$

3.2. Dynamic Performance Optimization

In the suspension optimization process, assuming that the vehicle is driving at a speed of u = 20 m/s on a Class C road, the input displacement of road roughness can be expressed as follows:

$$\dot{z}_r(t) = -0.111[uz_r(t) + 40\sqrt{G_q(n_0)u}w(t)] \quad (14)$$

where $z_r(t)$ is the vertical input displacement caused by the road roughness of the model; $Gq(n_0)$ is the road roughness coefficient, with a value of 2.56×10^{-4} m; $w(t)$ denotes integral white noise.

(1) Pigeon-inspired optimization

Optimization algorithms include single-objective optimization algorithms and multi-objective optimization algorithms [28]. The objective of this paper is to optimize body acceleration. Therefore, a single-objective optimization algorithm, pigeon-inspired optimization (PIO), is adopted.

Pigeon-inspired optimization (PIO) [29] is an intelligent optimization algorithm inspired by the homing behavior of pigeons. It has the advantages of global optimality and fast convergence. The PIO optimization algorithm simulates the homing behavior of pigeons based on magnetic field direction and landmarks to achieve the optimization process. The PIO algorithm can be roughly divided into two stages: the magnetic field operator and the landmark operator. During the stage of magnetic field operation, pigeons used the solar height and geomagnetic field as navigation tools in their homing behavior when they were far away from their destination. During the landmark operator stage, the landmark is used as a homing navigation tool, because the ground objects can be observed when the pigeons are close to the destination. The flow chart of the optimization process is shown in Figure 3.

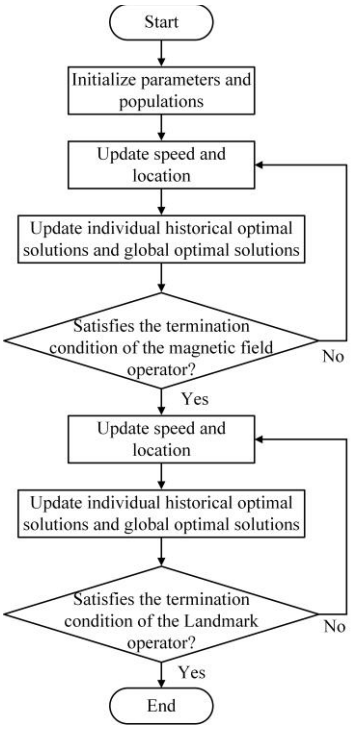


Figure 3. Algorithm flow chart.

In the D-dimensional search space, the initial pigeon population is N_p, and the position $X_{i(k)}$ and velocity $V_{i(k)}$ of the i-th pigeon in k iterations can be expressed as:

$$X_i(k) = [x_{i1}, x_{i2}, \cdots x_{iD}] \tag{15}$$

$$V_i(k) = [v_{i1}, v_{i2}, \cdots v_{iD}] \tag{16}$$

In the magnetic field operator stage, the positions $X_{i(k+1)}$ and velocities $V_{i(k+1)}$ of all pigeons at the next iteration $(k+1)$ can be updated using the following equation:

$$V_i(k+1) = V_i(k)e^{-Rk} + rand(X_g - X_i(k)) \tag{17}$$

$$X_i(k+1) = X_i(k) + V_i(k+1) \tag{18}$$

In Equation (17), R represents the magnetic field factor, rand is a uniformly distributed random number in the range [0,1], and X_g represents the global optimal solution of the current iteration. All pigeons adjust their flight positions according to magnetic field factors, and their positions are assessed using a specific objective function. Assuming that the maximum number of iterations of the magnetic field operator stage is nc1, if the current iteration t exceeds nc_1, the magnetic field operator stage is terminated and the landmark operator stage is entered.

During the landmark operator phase, all pigeons are sorted according to their fitness values. In each iteration, the number of pigeons is updated using Equation (19). Only half of the pigeons are taken into account when calculating the desired position of the central pigeon, while the remaining pigeons adjust their destination by following the desired target position. The position of the ideal destination is calculated using Equation (20), while all other pigeons are updated using Equation (21).

$$N_p(k+1) = \frac{N_p(k)}{2} \tag{19}$$

In Equation (19), $N_p(k)$ represents the number of pigeons at the current iteration k.

$$X_c(k+1) = \frac{\sum X_i(k+1) Fitness(X_i(k+1))}{N_p \sum Fitness(X_i(k+1))} \tag{20}$$

$$X_i(k+1) = X_i(k) + rand(X_c(k+1) - Xi(k)) \tag{21}$$

In Formulas (20) and (21), X_c is the desired position of the central pigeon, and $Fitness(\cdot)$ represents the fitness function of individual pigeons. Assuming that the maximum number of iterations of the landmark operator phase is nc_2, if the current iteration k exceeds nc_2, the landmark operator phase is aborted. The global optimal solution X_g is achieved by updating the optimal position in each iteration.

(2) Optimize objectives and constraints

In this paper, the optimization objectives for the vehicle ISD suspension model include the spring stiffness k_i, inertial coefficient b, maximum adjustable damping coefficient $c_{\max}$ and minimum adjustable damping coefficient $c_{\min}$. With comfort as the guide, the RMS of body acceleration under the road input, as shown in Equation (14), is taken as the optimization objective. The specific expression is shown below:

$$q = [k_i \; b \; c_{\max} \; c_{\min}] \tag{22}$$

$$\min J = J_1 \tag{23}$$

where J_1 represents the RMS of body acceleration of power-driven-damper vehicle ISD suspension under random road input; q represents the set of suspension parameters to be optimized.

This paper establishes certain constraints. J_1 should be less than J_{pass}, which represents the RMS of body acceleration in traditional passive suspension. It is relatively straightforward to calculate J_{pass}, which is equal to 1.607 m/s^2. In order to maintain the integrity of suspension working space and dynamic tire load during the optimization process, the following constraints are imposed [30]: Based on the probability integral table of the normal distribution, if the effective value of the suspension working space is less than or equal to 1/3 of the suspension dynamic deflection $[f_d]$, the probability of the suspension working space exceeding the limit travel is only 0.3%. For the passenger car studied in this paper, the range of $[f_d]$ is 7~9 cm, which is taken as 8 cm in this paper. For the dynamic tire load, when its effective value does not exceed 1/3 of the static load G, the probability of the wheel jumping off the ground does not exceed 0.15%. The static load G studied in this

paper is 3650 N. Since the main spring is the primary support of the suspension, the value range is set at [15,000, 25,000] $N \cdot m^{-1}$.

In summary, the optimization constraints are as follows:

$$s.t. \begin{cases} J_1 \leq J_{pass} \\ J_2 \leq \frac{f_d}{3} \\ J_3 \leq \frac{G}{3} \\ c_{\max}, c_{\min} \in [0,\ 10{,}000] \\ k_1 \in [10{,}000,\ 25{,}000], k_2, k_3, k_4 \in [0,\ 10{,}000] \\ b_2 \in [0,\ 4000] \end{cases} \tag{24}$$

The parameters of the passenger car in this paper are shown in Table 1, and the final optimization results are shown in Table 2 [31]. The suspension S0 represents the traditional passive suspension.

Table 1. Passenger of car parameter.

Parameters	Symbol	Unit	Value
Sprung mass	m_s	kg	320
Unsprung mass	m_u	kg	45
Support spring stiffness	K	$N \cdot m^{-1}$	22,000
Damper coefficient	C	$N \cdot s \cdot m^{-1}$	1000
Tire stiffness	k_t	$N \cdot m^{-1}$	190,000
Speed of vehicle	u	$m \cdot s^{-1}$	20
Grade C Road roughness coefficient	$G_q(n_0)$	$m^3 \cdot cycle^{-1}$	2.56×10^{-4}

Table 2. The results of the optimal design.

Layouts	Optimized Parameters	J_1	J_2	J_3
S0	k_1 = 22,000, C = 1000	1.607	0.0169	1150.3
S1	k_1 = 15,160, b = 16, $c_{\max}$ = 9293, $c_{\min}$ = 1025	1.4247(11.4%↓)	0.0139(17.8%↓)	1216.7
S2	k_1 = 15,337, k_2 = 2544, b = 5, $c_{\max}$ = 9617, $c_{\min}$ = 750	1.3883(13.7%↓)	0.0152(9.5%↓)	1216.7
S3	k_1 = 15,128, k_2 = 9814, k_3 = 2122, b = 1936, $c_{\max}$ = 9817, $c_{\min}$ = 777	1.2986(20.0%↓)	0.0163(3.6%↓)	1216.7
S4	k_1 = 15,011, k_2 = 7424, k_3 = 9778, k_4 = 5, b = 3665, $c_{\max}$ = 9961, $c_{\min}$ = 788	1.2359(23.1%↓)	0.0158(6.6%↓)	1216.7

As shown in Table 2, the body acceleration is improved after optimizing all structures, and the improvement is more significant as the structure becomes more complex. It is worth noting that the suspension working space is also improved, while the dynamic tire load deteriorates to some extent. This is because optimizing body acceleration may lead to some extent of deterioration in other dynamic performance indicators. When the optimization process concludes, the dynamic tire load reaches the constraint boundary, but its value remains within a reasonable range.

The suspension S4 has achieved the most significant improvement in body acceleration, with a 23.1% decrease in body acceleration. The suspension working space of suspension S1 has been significantly improved, with a 17.8% decrease in suspension working space. However, the body acceleration of suspension S1 has only decreased by 11.4%. The body acceleration of suspension S2 and suspension S3 decreased by 13.7% and 20.0%,

respectively. However, the improvement is not as significant as that of suspension S4. This paper is comfort-oriented, the body acceleration can directly reflect whether the ride comfort is excellent. Compared to other suspensions, the suspension S4 has the best effect on improving body acceleration. Therefore, the suspension S4 was chosen as the research object to analyze its dynamic characteristics.

4. Dynamic Performance Analysis

4.1. Influence of Damping Coefficient Variation on Dynamic Performance

The primary goal of the power-driven-damper control strategy is to regulate the damping adjustment in order to improve the dynamic performance of the suspension. In order to further study the action mechanism of the power-driven-damper vehicle ISD suspension, this study analyzes the influence of the damping coefficient on body acceleration, suspension working space, and dynamic tire load. The maximum damping coefficient c_{max} and the minimum damping coefficient c_{min} of the power-driven-damper control strategy are set at 0–10,000 N·s/m and 0–2000 N·s/m, respectively, and this analysis is based on the optimized suspension structure parameters. The simulation results are shown in Figure 4, where the star symbol represents optimal value point.

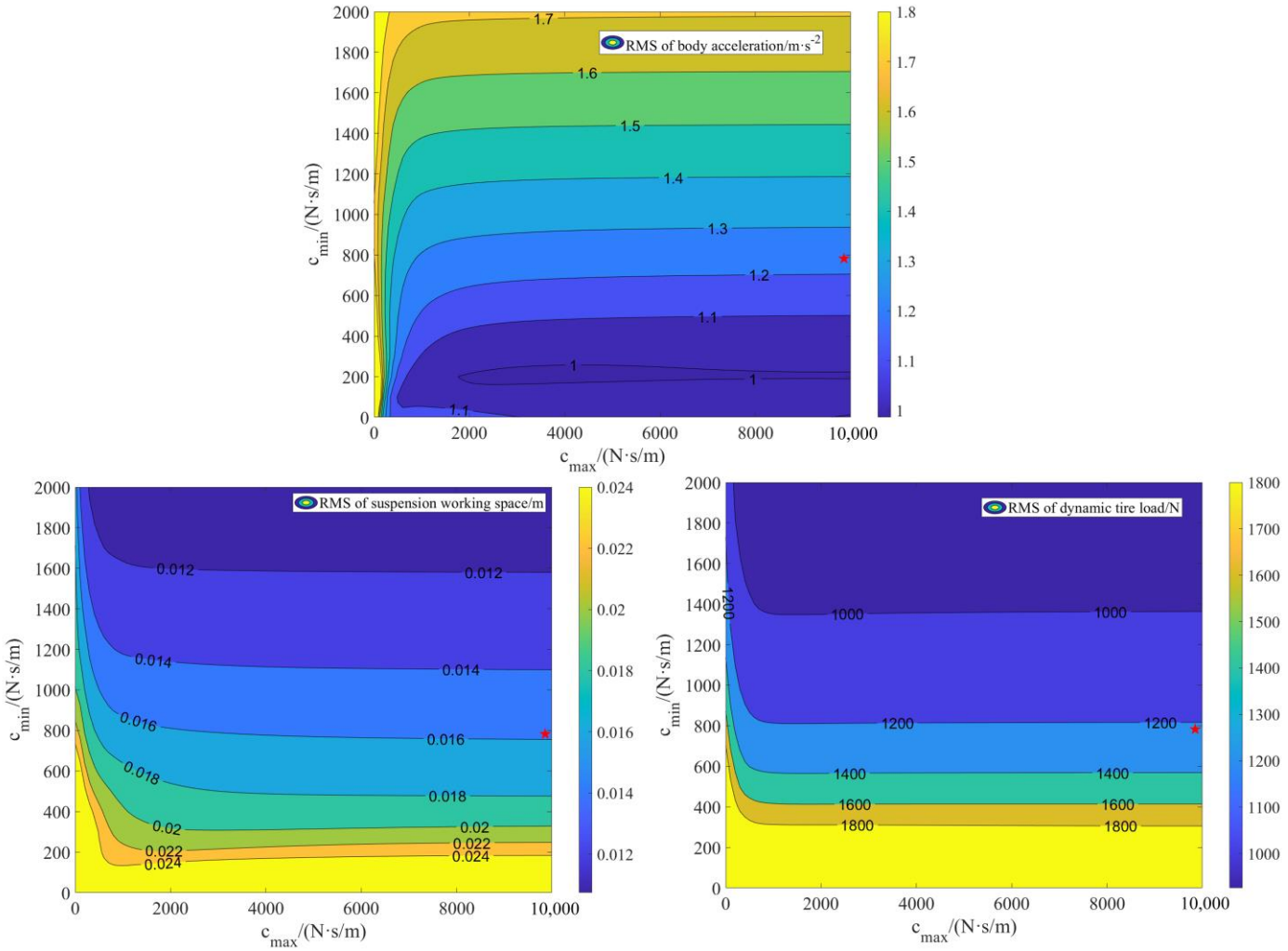


Figure 4. Dynamic performance contour map.

From Figure 4, it can be seen that, as the c_{min} increases, the RMS of body acceleration initially decreases and then increases. As the c_{max} increases, the RMS of body acceleration gradually decreases. Therefore, when the c_{min} is around 200 N·s·m^{-1} and the c_{max} reaches

the upper limit, the RMS of body acceleration is minimum. However, we need to consider that the RMS of suspension working space and the dynamic tire load are both within an acceptable range. For the variation of the RMS of suspension working space, as c_{min} increases, the RMS of suspension working space gradually decreases. As c_{max} increases, the RMS of suspension working space gradually decreases. Therefore, when both c_{max} and c_{min} reach the upper limit, the RMS of suspension working space is minimum. For the variation of the RMS of dynamic tire load, as the c_{min} increases, the RMS of dynamic tire load gradually decreases. As the c_{max} increases, the RMS of dynamic tire load rapidly decreases and then tends to converge. Therefore, when the c_{min} reaches the upper limit and the c_{max} is relatively large, the RMS of dynamic tire load is minimum.

4.2. Research on Vibration Suppression Mechanism in Wide Frequency Domain

Suspension S4 is selected as the research object, and the suspension structure parameters are set according to the optimized parameters in Table 2. The body acceleration gain of the S4 suspension is obtained through simulation, as shown in Figure 5. From Figure 5, it can be seen that in the low frequency range, the amplitude of the body acceleration gain for suspension S4 has significantly decreased compared to that of suspension S0. In the high frequency range, the amplitude of the body acceleration gain has also decreased to some extent. The body acceleration gain of suspension S4 is smaller than that of suspension S0 in the range of 0–15 Hz. It can be inferred that, by combining ISD suspension and power-driven-damper control strategy, the suspension can effectively inherit the low-frequency vibration suppression effect of ISD suspension and the high-frequency vibration suppression effect of the power-driven-damper control strategy. Thus, it can be concluded that the power-driven-damper vehicle ISD suspension has a broadband vibration suppression characteristic.

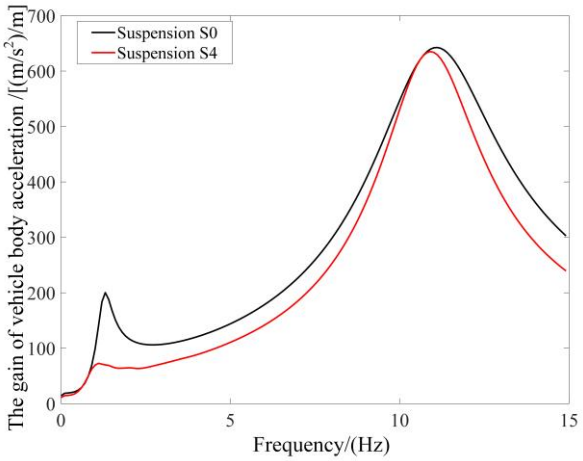


Figure 5. Gain of body acceleration comparison diagram.

4.3. Time Domain Simulation

A random pavement model with a grade of C is selected as the input excitation, as shown in Equation (14). The simulation results of body acceleration, suspension working space, and dynamic tire load at a vehicle speed of 20 m/s are shown in Figure 6. From Figure 6, it is evident that suspension S4 exhibits significantly improved body acceleration performance compared to suspension S0 throughout the simulation period. Additionally, the suspension working space has also been improved to some extent. However, the dynamic tire load has deteriorated compared to the S0 suspension. This is due to sacrificing of dynamic tire load in order to improve body acceleration. However, the dynamic tire load still remains within a reasonable range.

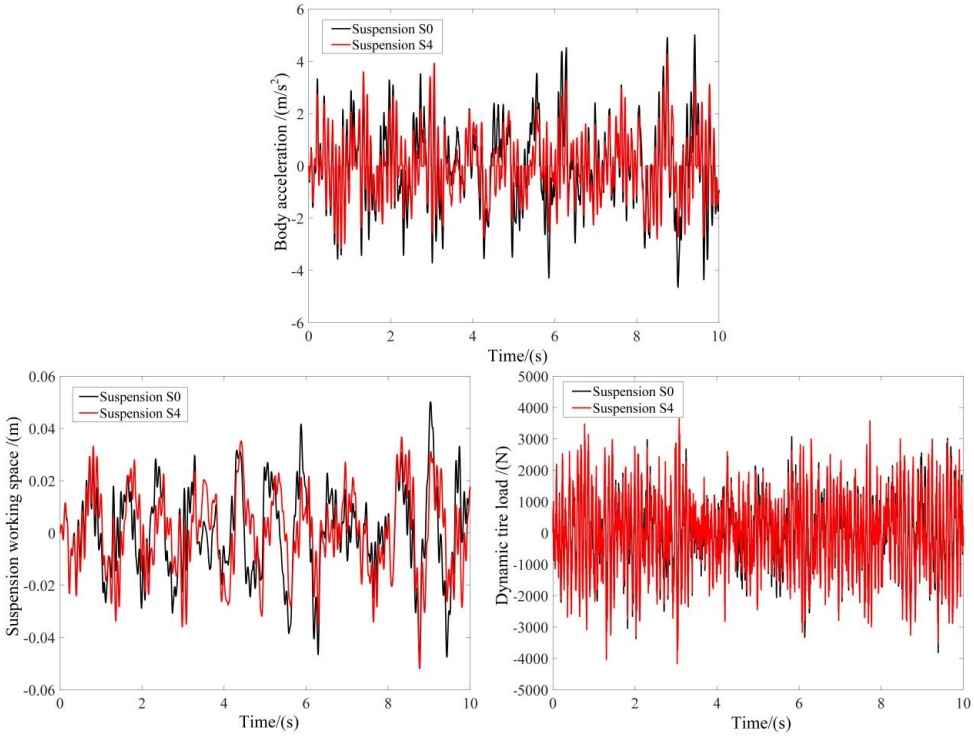


Figure 6. Time-domain comparison of suspension performance.

4.4. Frequency Domain Simulation

In order to further analyze the vibration suppression mechanism of power-driven-damper vehicle ISD suspension, Fourier series transformations are used to convert the time-domain diagram into the frequency-domain diagram, as shown in Figure 7.

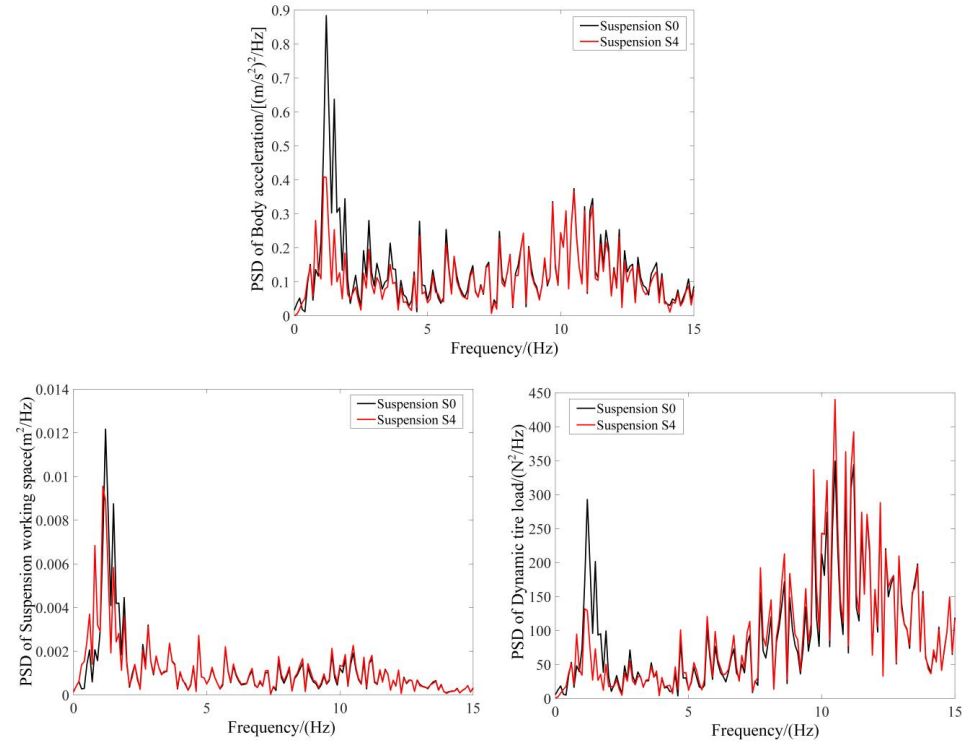


Figure 7. Frequency-domain comparison of suspension performance.

From Figure 6, it can be seen that compared to suspension S0, the power spectral density of body acceleration of suspension S4 has improved in the 0–15 Hz range, with significant improvements in the low-frequency range of 5 Hz and below. This study examines the characteristics of power-driven-damper vehicle ISD suspension, which can improve body acceleration and suppress vibration over a broad frequency range. The power spectral density of suspension working space of suspension S4 deteriorates within the 1 Hz range but is nearly consistent with that of suspension S0 in the frequency band of 2 Hz and higher. However, there is a significant improvement between 1 Hz and 2 Hz. The power spectral density of dynamic tire load of Suspension S4 has significantly improved between 2 Hz and 4 Hz.

4.5. Discussion of the Results

From the above analysis, it can be seen that the RMS of body acceleration, suspension working space, and dynamic tire load are affected differently by the damping coefficient. However, the general trend indicates that body acceleration is inversely related to suspension working space and dynamic tire load. This means that while improving body acceleration, the other two performance indicators will deteriorate. The body acceleration gain of suspension S4 has been improved in the range of 0–15 Hz compared to suspension S0, which reflects the broadband vibration suppression characteristics of the power-driven-damper vehicle ISD suspension. The analysis in both the time-domain and frequency-domain shows that the body acceleration of suspension S4 is significantly improved compared to suspension S0. This improvement effectively enhances the ride comfort. The suspension S4 proposed in this paper effectively applies power-driven-damper control strategy to the ISD suspension. This approach achieves broadband vibration suppression and significantly improves body acceleration. In comparison to other suspensions, it achieves broadband vibration suppression without producing jitter.

5. Conclusions

In this paper, a quarter suspension model is established. Firstly, the expression of the power-driven-damper control strategy applied to vehicle ISD suspension is solved based on port-controlled Hamiltonian theory. Then, the suspension structure is topologically designed, four suspension structures are obtained, and the pigeon-inspired optimization is used to optimize the four structural parameters. Based on random road input, simulation results show that suspension S4 has reduced body acceleration by 23.1% compared to suspension S0, making it the most effective among all suspensions. This paper is comfort-oriented, and body acceleration directly affects the quality of riding comfort. Therefore, we selected suspension S4 as the research object. Based on the suspension S4, this study analyzes the impact of the damping coefficient on the performance of the power-driven-damper vehicle ISD suspension. We also analyze the variations in body acceleration gain and dynamic characteristics in both the time-domain and frequency-domain. The results show that, under the random input condition, the suspension S4 can decrease the RMS of body acceleration and the RMS of suspension working space by 23.1% and 6.6%, respectively, compared to the suspension S0 (traditional passive suspension), which effectively improves the ride comfort of the vehicle. The contour of body acceleration, suspension working space, and dynamic tire load reveal the impact of changes in damping coefficient on suspension dynamic performance. Both time-domain and frequency-domain analyses show that the power-driven-damper vehicle ISD suspension can effectively decrease body acceleration and significantly improve ride comfort.

The power-driven-damper vehicle ISD suspension designed in this paper achieves broadband vibration suppression without jitter associated with ADD control and without complex switching conditions. The variously designed structures lead to significant performance differences. The power-driven-damper vehicle ISD suspension, based on the optimum structure, significantly reduces body acceleration and effectively improves ride comfort. The optimization design method of suspension structures in this article

presents new ideas for the structural design of suspensions. The broadband vibration suppression characteristics of the power-driven-damper vehicle ISD suspension offer a research direction for suppressing suspension vibration.

This paper exclusively focuses on conducting research using the quarter suspension model. However, it is also worth considering exploring high-dimensional dynamic models, such as the half vehicle and whole vehicle models. This article focuses solely on simulation analysis. Future research will include experiments to validate the simulation results.

Author Contributions: Conceptualization, Y.S.; methodology, X.Y.; software, J.W.; validation, J.W., F.D. and M.L.; formal analysis, F.D.; investigation, Y.S.; resources, M.L.; data curation, J.W.; writing—original draft preparation, J.W.; writing—review and editing, J.W.; visualization, Y.S.; supervision, X.Y.; project administration, Y.S.; funding acquisition, Y.S. All authors have read and agreed to the published version of the manuscript.

Funding: This research was funded by the National Natural Science Foundation of China under Grant 52002156 and 52072157, Postgraduate Research & Practice Innovation Program of Jiangsu Province (Grant No. SJCX22_1850) and Young Elite Scientists Sponsorship Program by CAST (No. 2022QNRC001).

Data Availability Statement: Data are contained within the article.

Acknowledgments: The authors would like to thank the editor and the anonymous reviewers for their careful reading and helpful comments.

Conflicts of Interest: Ming Li is employee of Weichai (Yangzhou) Yaxing New Energy Commercial Vehicle Co., Ltd. The paper reflects the views of the scientists, and not the company. The authors declare no conflicts of interest.

Abbreviations

Abbreviation	Meaning
ISD	Inerter-Spring-Damper
PDD	Power-driven-damper
ADD	Acceleration-driven-damper
SH	Skyhook
LQR	Liner-quadratic-regulator

References

1. Wen, X.; Li, Y.N.; Yang, C. Design, Modeling, and Characterization of a Tubular Linear Vibration Energy Harvester for Integrated Active Wheel System. *Automot. Innov.* **2021**, *4*, 413–429. [CrossRef]
2. Sun, W.C.; Zhang, J.H.; Pan, H.H. Heavy vehicle air suspension control considering ride comfort and height regulation. *Control Theory Appl.* **2022**, *39*, 1002–1010.
3. Qin, Y.Z.; Zhao, Z.; Wang, Z.F.; Li, G.F. Study of Longitudinal–Vertical Dynamics for In-Wheel Motor-Driven Electric Vehicles. *Automot. Innov.* **2021**, *4*, 227–237. [CrossRef]
4. Issa, M.; Samn, A. Passive vehicle suspension system optimization using Harris Hawk Optimization algorithm. *Math. Comput. Simul.* **2021**, *191*, 328–345. [CrossRef]
5. Kumar, S.; Medhavi, A.; Kumar, R. Optimization of Nonlinear Passive Suspension System to Minimize Road Damage for Heavy Goods Vehicle. *Int. J. Acoust. Vib.* **2021**, *26*, 56–63. [CrossRef]
6. Abut, T.; Salkim, E. Control of Quarter-Car Active Suspension System Based on Optimized Fuzzy Linear Quadratic Regulator Control Method. *Appl. Sci.* **2023**, *13*, 8802. [CrossRef]
7. Nie, J.; Wang, F.; Zhang, X.; Yang, Y. Design and test of hydro-pneumatic ISD suspension in heavy multi-axle vehicles. *Adv. Mech. Eng.* **2021**, *13*, 16878140211064737. [CrossRef]
8. Wang, K.; Chen, M.Z.Q.; Li, C.; Chen, G. Passive Controller Realization of a Biquadratic Impedance with Double Poles and Zeros as a Seven-Element Series-Parallel Network for Effective Mechanical Control. *IEEE Trans. Autom. Control* **2018**, *63*, 3010–3015. [CrossRef]
9. Li, F.J.; Li, X.P.; Shang, D.Y.; Wang, Z. Dynamic modeling and damping performance improvement of two stage ISD suspension system. *Proc. Inst. Mech. Eng. Part D J. Automob. Eng.* **2022**, *236*, 2259–2271. [CrossRef]
10. Chen, L.; Zhang, X.L.; Nie, J.M.; Wang, R.C. Performance Analysis of Two-stage Series-connected Inerter-spring-damper Suspension Based on Half-car Model. *J. Mech. Eng.* **2012**, *48*, 102–108. [CrossRef]

11. Du, F.; Mao, M.; Chen, Y.J.; Wang, Y.J.; Zhang, Y.F. Structure design and performance analysis of inerter-spring-damper suspension structure based on dynamic model and parameter optimization. *J. Vib. Shock* **2014**, *33*, 59–65.
12. Xu, L.; Mao, M.; Chen, Y.J.; Du, F. Configuration Design and Analysis of two-stage tandem ISD suspension. *J. Ordnance Equip. Eng.* **2020**, *41*, 7–12.
13. Nie, J.M.; Zhang, X.L.; Sun, X.Q.; Wang, R.C. Modeling and Parameter Optimization of a New Hybrid ISD Suspension. *Automot. Eng.* **2015**, *2*, 44–47.
14. Paageorgiou, C.; Smith, M.C. Positive real synthesis using matrix inequalities for mechanical networks: Application to vehicle suspension. *IEEE Trans. Control Syst. Technol.* **2006**, *14*, 423–435. [CrossRef]
15. Jiang, J.Z.; Smith, M.C. Series-Parallel Six-Element Synthesis of Biquadratic Impedances. *IEEE Trans. Circuits Syst. I Regul. Pap.* **2012**, *59*, 2543–2554. [CrossRef]
16. Zhang, S.Y.; Jiang, J.Z.; Neild, S.A. Passive vibration control: A structure-immittance approach. *Proc. R. Soc. A Math. Phys. Eng. Sci.* **2017**, *473*, 20170011.
17. Ioan-Cozmin, M.R.; Cornel, S.; Ioan, M. Analysis of passive vs. semi-active quarter car suspension model. In Proceedings of the Conference on Advanced Topics in Optoelectronics, Microelectronics and Nanotechnologies, Constanta, Romania, 20–23 August 2020; p. 11718.
18. Jayaraman, T.; Palanisamy, S.; Thangaraj, M. Hydraulic control valve integrated novel semi active roll resistant interconnected suspension with vertical and roll coordinated control scheme. *Proc. Inst. Mech. Eng. Part D-J. Automob. Eng.* **2022**, *237*, 98–111. [CrossRef]
19. Ma, T.; Bi, F.; Wang, X.; Tian, C.; Lin, J.; Wang, J.; Pang, G. Optimized Fuzzy Skyhook Control for Semi-Active Vehicle Suspension with New Inverse Model of Magnetorheological Fluid Damper. *Energies* **2021**, *14*, 1674. [CrossRef]
20. Karnopp, D.; Crosby, M.J.; Harwood, R.A. Vibration control using semi-active force generators. *J. Eng. Ind.* **1974**, *96*, 619–626. [CrossRef]
21. Karnopp, D.; Crosby, M.J. The active damper a new concept for shock and vibration control. *Shock Vib. Bull.* **1973**, *143*, 119–133.
22. Zhu, B.L.; Qing, W.; ShangGuan, W.B.; Rakheja, S. Modeling and control of a quarter-car model with double wishbones and its equivalent two degrees of freedom model. *J. Vib. Shock* **2019**, *10*, 6–14.
23. Lin, C.B.; Wang, Y.; Xu, E.Y.; Liu, F.Y.; Zhao, L.L.; Tang, Z.T. Study on improved ADD control Strategy for semi-active Suspensions. *Noise Vib. Control* **2023**, *43*, 197–202.
24. Wang, Y.; Liu, F.Y.; Deng, J.C.; Zhao, L.L.; Tang, Z.T. Simulation Analysis of SH-LQR Damping Control Strategy for Semi-active Suspensions. *Noise Vib. Control* **2022**, *42*, 68–72.
25. Savaresi, S.M.; Spelta, C. Mixed Sky-Hook and ADD: Approaching the Filtering Limits of a Semi-Active Suspension. *J. Dyn. Syst. Meas. Control* **2007**, *129*, 382–392. [CrossRef]
26. Liu, Y.L.; Zuo, L. Mixed Skyhook and Power-Driven-Damper: A New Low-Jerk Semi-Active Suspension Control Based on Power Flow Analysis. *J. Dyn. Syst. Meas. Control* **2016**, *138*, 081009. [CrossRef]
27. Morselli, R.; Zanasi, R. Control of port Hamiltonian systems by dissipative devices and its application to improve the semi-active suspension behaviour. *Mechatronics* **2008**, *18*, 364–369. [CrossRef]
28. Talebitooti, R.; Gohari, H.D.; Zarastvand, M.R. Multi objective optimization of sound transmission across laminated composite cylindrical shell lined with porous core investigating Non-dominated Sorting Genetic Algorithm. *Aerosp. Sci. Technol.* **2017**, *69*, 269–280. [CrossRef]
29. Qiu, H.X.; Duan, H.B. Multi-objective pigeon-inspired optimization for brushless direct current motor parameter design. *Sci. China-Technol. Sci.* **2015**, *58*, 1915–1923. [CrossRef]
30. Sun, X.Q.; Chen, L.; Wang, S.H. Nonlinear modeling and parameter optimization of two-stage series ISD suspension. *Trans. Chin. Soc. Agric. Mach.* **2014**, *45*, 7–13.
31. Liu, Y.L.; Yan, L.; Yang, X.F.; Shen, Y.; Liu, C. Optimization design and performance of vehicle ISD suspension based on ADD positive real network. *J. Vib. Shock* **2021**, *40*, 262–268.

Disclaimer/Publisher's Note: The statements, opinions and data contained in all publications are solely those of the individual author(s) and contributor(s) and not of MDPI and/or the editor(s). MDPI and/or the editor(s) disclaim responsibility for any injury to people or property resulting from any ideas, methods, instructions or products referred to in the content.